NJC

ROYAL SOCIETY OF CHEMISTRY

PAPER

Published on 22 September 2026
Licence and permissions

Check for updates

Cite this: DOI: 10.1039/d6nj02037b

A simple turn-off fluorescent sensing of trace Cu^{2+} using a PEI–vanillin imine network in aqueous media

Berly Robert, *[a] Mohanraj Jagannathan, [b] Moon Il Kim [b] and Sreeram K. Kalpathy *[ac]

Received 1st June 2026,
Accepted 31st July 2026

DOI: 10.1039/d6nj02037b

rsc.li/njc

Copper (Cu^{2+}) is an essential trace element involved in various enzymatic and physiological processes. However, it becomes toxic when accumulated beyond permissible limits. In this work, we report the design of a water-soluble, fluorescence-responsive sensor based on a Schiff base formed through the condensation of polyethylenimine (PEI) and vanillin, a naturally derived aromatic aldehyde, engineered specifically for the selective recognition of Cu^{2+} ions in aqueous environments. The synthesized Schiff-base ligand was characterized by UV-Vis, FTIR, and ^{1}H NMR spectroscopy, while its interaction with Cu^{2+} was confirmed through fluorescence spectroscopy and XPS analysis. This method offers a remarkably simple and straightforward sensing strategy, using minimal synthetic steps and entirely aqueous processing. The sensor exhibited a distinct fluorescence response upon interaction with Cu^{2+}, attributed to coordination at the imine (–C═N–) site and vanillin donor groups. The system showed high selectivity toward Cu^{2+} over other competing metal ions in the 800–100 μM and 1000–10 nM regimes, with a limit of detection of 290 nM. The probe was synthesized *via* a simple aqueous-phase reaction between the sensing components to form fluorescent Schiff-base sites, eliminating the use of organic solvents, and it enabled sensitive and selective fluorescence-based detection of heavy-metal ions under ambient conditions. In addition to liquid phase sensing, the compatibility of the probe with porous substrates suggests the potential for the future development of portable paper-based detection platforms.

1 Introduction

Contamination of water resources by heavy metal ions (HMIs) remains a pressing global concern, with heavy metals such as lead, arsenic, mercury, and cadmium among the most common toxic species in aquatic environments.[1,2] Among these toxic metal ions, copper presents a unique challenge because it exhibits a dual nature as both an essential micronutrient and a potential environmental toxicant. Its widespread use in industrial, agricultural, and domestic applications significantly increases the risk of overexposure.[3,4] While Cu^{2+} ions serve critical functions in biological systems, particularly in enzymatic redox processes and oxygen activation through complex copper active sites,[5] their excessive accumulation has been associated with liver cirrhosis, kidney dysfunction, and neurodegenerative disorders.[6] Given its dual role as both a necessary micronutrient and a potential toxicant, the selective and eco-friendly detection of Cu^{2+} in aqueous environments is both scientifically and environmentally relevant. Therefore, maintaining copper concentrations within the permissible range is essential for protecting both environmental and public health. Recognizing the potential health risks associated with copper exposure, the World Health Organization (WHO) and the United States Environmental Protection Agency (USEPA) have set the maximum allowable limits for copper in drinking water at 2.0 mg L^{-1} and 1.3 mg L^{-1}, respectively.[7] The growing demand for real-time, cost-effective and field-deployable copper ion detection systems has therefore driven significant research to develop selective and sensitive sensing platforms, especially those that are environmentally benign and user-friendly.[8–10]

In recent years, various analytical techniques have been explored for HMI detection, among which optical approaches have gained considerable attention due to their operational simplicity, rapid response, and non-destructive characteristics. Fluorescence-based sensing, in particular, has emerged as a powerful strategy owing to its high sensitivity, real-time

[a] Department of Metallurgical and Materials Engineering, Indian Institute of Technology Madras, Chennai 600036, India. E-mail: berlyrobert87@gmail.com, ic40308@imail.iitm.ac.in, sreeram@iitm.ac.in
[b] Department of BioNano Technology, Gachon University, 1342 Seongnamdae-ro, Sujeong-gu, Seongnam-si, Gyeonggi-do 13120, Republic of Korea
[c] Centre for Resource Efficiency, Recyclability and Circularity in Energy Transition, School of Sustainability, Indian Institute of Technology Madras, Chennai 600036, India

monitoring capability, and adaptability to portable formats.[11] These sensors can detect target analytes through measurable changes in emission intensity, wavelength, or fluorescence lifetime, enabling sensitive monitoring even at trace concentrations. Owing to these advantages, a diverse range of fluorescent materials, including organic dyes, rare-earth complexes, metal–organic frameworks (MOFs), semiconductor quantum dots, metallic nanoparticles, and carbon-based quantum dots, have been investigated for HMI sensing applications.[12–15] Among these, MOF-based fluorescent sensors have attracted significant attention because of their high surface area, tunable pore structures, excellent chemical stability, and intrinsic luminescent properties, enabling highly selective and sensitive detection of a wide range of analytes. Recent studies have demonstrated that rationally designed luminescent MOFs can achieve nanomolar detection limits with excellent selectivity, anti-interference capability, and recyclability through mechanisms such as photoinduced electron transfer (PET), the inner filter effect (IFE), and competitive absorption (CA). These advances highlight the growing potential of MOFs as versatile fluorescent sensing platforms for environmental monitoring and biomedical analysis.[16–20]

In parallel, considerable progress has also been achieved using ratiometric fluorescent probes, FRET-based sensing systems, graphene-assisted fluorescence amplification, and near-infrared fluorescent probes, which significantly improve sensing accuracy by minimizing background interference and enhancing signal reliability.[21–23] These advanced fluorescence strategies have enabled ultrasensitive detection of diverse biomarkers and pollutants while expanding the applicability of fluorescence sensing to biological imaging, food safety, and environmental monitoring. Despite their promising analytical performance, several of these systems suffer from drawbacks such as complicated synthesis routes, poor water solubility, or reliance on expensive and non-biodegradable components. Furthermore, many recently reported fluorescence probes are primarily designed for biomedical imaging or specific molecular biomarkers rather than routine heavy metal monitoring in aqueous environments. Consequently, increasing attention has been directed toward developing simple, structurally tunable, water-compatible, and environmentally benign molecular platforms for selective heavy metal ion detection.

Among the numerous molecular fluorophores explored for metal ion sensing, Schiff bases have attracted considerable interest as fluorescent chemosensors due to their straightforward synthesis *via* condensation of amines and aldehydes, structural versatility, and strong metal-chelating ability.[24,25] Schiff bases often exhibit fluorescence due to π–π^* transitions originating from their extended conjugated π-electron system formed by the imine (C═N) bond and aromatic moieties.[26–28] In addition, the presence of azomethine (C═N) groups along with additional donor sites such as phenolic –OH groups enables efficient coordination with transition metal ions, often resulting in measurable fluorescence modulation.[29,30] Numerous Schiff base-based probes have been reported for selective metal ion detection.[31–33] Nevertheless, most reported Schiff base sensors for HMI detection are derived from synthetic aldehydes[34–36] or are based on low molecular weight fluorophores, which often exhibit limited aqueous stability and reduced processability and comparatively lower suitability for practical sensing applications. This underexplored area highlights an important opportunity for the development of environmentally benign and practically viable Schiff base sensing materials.[37]

To overcome these limitations, integrating Schiff base functionality into polymeric frameworks has emerged as an effective strategy to enhance stability, water compatibility, metal-binding density, enhanced selectivity and sensitivity toward target metal ions.[38–40] Among various polymeric matrices, polyethyleneimine (PEI) has emerged as an attractive platform because of its highly branched structure, excellent water solubility, biocompatibility, and exceptionally high amine density. PEI readily undergoes condensation with aldehydes to form Schiff base linkages in solution.[41–43] The abundance of primary, secondary, and tertiary amines in PEI enables rapid imine formation and provides multiple coordination sites for metal ions, thereby enhancing the binding efficiency and signal responsiveness.[41] Furthermore, its excellent film-forming ability, biocompatibility, and fast response characteristics make PEI-based systems promising for real-time environmental monitoring applications.[35]

Beyond the incorporation of Schiff base functionality into polymeric frameworks, the choice of aldehyde component plays a crucial role in modulating the optical and coordination properties of the resulting Schiff base. While several studies have employed synthetic aldehydes such as salicylaldehyde (SA), 2-hydroxy-1-naphthaldehyde, and other fluorophore-containing derivatives for PEI-based sensing systems, these materials are often commercially sourced and less environmentally sustainable.[35,44] For example, Tan *et al.* developed a PEI-SA system for Zn^{2+} and Cd^{2+} detection, though it required additional reagents for ion differentiation and exhibited limited selectivity.[44] Mondal and Dey reported PEI-based fluorescent composites derived from aldehydes such as 4-hydroxybenzaldehyde, 2-hydroxynaphthaldehyde, and SA, demonstrating ion-dependent fluorescence responses; however, the systems relied on synthetic aldehydes.[35,36] Similarly, Fan *et al.* fabricated a solid-phase sensor through multi-step surface modification involving PEI and salicylaldehyde, which, despite its effectiveness, required chemical pre-treatment and sequential processing steps.[34] Relatively few studies have explored naturally derived aldehydes for constructing environmentally sustainable polymeric fluorescent probes capable of direct Cu^{2+} detection in aqueous media.

In this regard, vanillin, a naturally derived aromatic aldehyde, offers a sustainable and biocompatible alternative. Its aldehyde functionality readily forms imine bonds with amine-containing compounds, while the phenolic group promotes electron delocalization and provides favorable sites for metal ion interaction.[45,46] Zhao *et al.* demonstrated that vanillin-derived polymers can undergo efficient Schiff base reactions under mild conditions, enabling functional material development.[47] Kumar *et al.*

 This journal is © The Royal Society of Chemistry and the Centre National de la Recherche Scientifique 2026

reported vanillin-based Schiff bases capable of forming stable coordination complexes with metal ions, achieving high extraction efficiencies.[48] These findings suggest that vanillin-based Schiff bases can provide strong coordination ability while maintaining environmental compatibility. Based on this rationale, we designed a green, liquid-phase sensing platform by combining PEI and vanillin to spontaneously form a Schiff base in aqueous media. The resulting PEI–vanillin probe leverages the high amine density of PEI and the phenolic-imine coordination sites of vanillin to achieve selective fluorescence quenching in the presence of Cu^{2+}. A schematic depicting this typical reaction is presented in Fig. 1.

To further demonstrate its practical applicability, the synthesized PEI–vanillin probe was immobilized onto cellulose-based Whatman filter paper (WFP) through a straightforward drop-casting process to fabricate disposable paper-based sensing strips. The resulting platform exhibited selective fluorescence quenching and distinct visual responses toward Cu^{2+} demonstrating its suitability for rapid on-site monitoring. The combination of sustainable molecular design, aqueous synthesis, polymeric stability, and portable paper-based implementation distinguishes the present work from previously reported Schiff base and polymeric fluorescent sensing systems. Furthermore, the development of environmentally benign fluorescent sensors for heavy metal monitoring contributes directly toward several United Nations Sustainable Development Goals (SDGs), notably SDG 6 (Clean Water and Sanitation), SDG 3 (Good Health and Well-being), and SDG 12 (Responsible Consumption and Production), by enabling fast and precise detection of toxic metal pollutants in water, thereby contributing towards better public health and environmental protection.

2 Materials and methods

2.1 Materials

Polyethylenimine (PEI, branched, average M_w ~25 000, M_n ~10 000; CAS No. 9002-98-6) was purchased from Merck. Vanillin (extrapure AR, 99%, 4-hydroxy-3-methoxybenzaldehyde; MW 152.15, $C_8H_8O_3$) was purchased from SRL. Solutions of Cu^{2+}, Cd^{2+}, Cr^{3+}, Co^{2+}, Fe^{3+}, Zn^{2+}, Mn^{2+}, Al^{3+}, Pb^{2+}, Hg^{2+}, and Ni^{2+} were prepared from cupric chloride (170.48), cadmium chloride (183.32), chromium(III) nitrate (400.15), cobalt(II) nitrate (291.03), iron(III) chloride hexahydrate (270.30), zinc sulphate heptahydrate (287.54), manganese(II) chloride tetrahydrate (197.90), aluminium chloride hexahydrate (241.43), lead(II) nitrate (331.21), mercuric chloride (271.50) and nickel(II) chloride hexahydrate (237.7), respectively. Deionized (DI) water with a specific conductance below 1 S cm^{-1} at 25 °C (specific gravity 1.0) was procured from Nice Chemicals Pvt. Ltd, India. All the reagents (solvents and chemicals) were used without any additional purification.

2.2 Synthesis of the polyethylenimine and vanillin-based Schiff base

The Schiff base-based liquid sensor material was prepared by reacting PEI with vanillin through imine bond formation between the amine groups of PEI and the aldehyde group of vanillin. Briefly, PEI (0.5 g, 1.0 wt%) was dissolved in 50 mL of deionized water under continuous stirring for 60 min to obtain a homogeneous solution. Subsequently, vanillin (25 mg, 0.05 wt%) was added to the PEI solution, maintaining a PEI molar ratio of 1 : 8, and the reaction mixture was stirred continuously for 3 h at room temperature to facilitate Schiff base formation. No additional pH adjustment was performed,

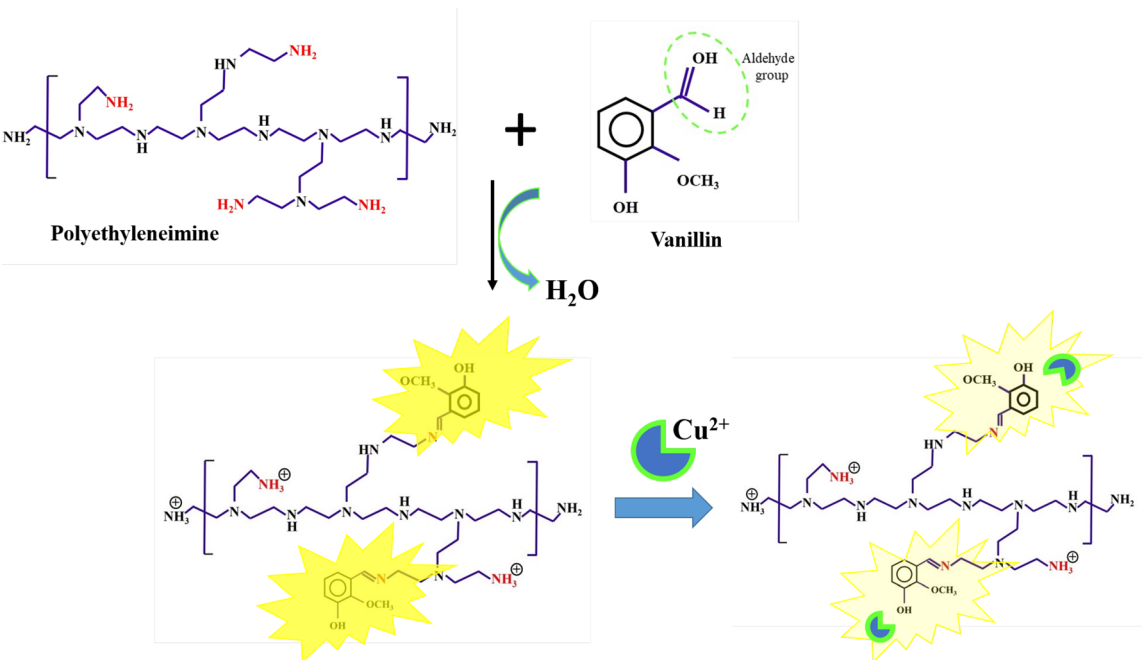


Fig. 1 PEI and vanillin Schiff base reaction mechanism.

and the reaction was carried out under the inherent pH conditions of the PEI–vanillin system. The obtained PEI–vanillin Schiff base solution was stored at room temperature under light-protected conditions by wrapping the container with aluminum foil. For characterization and HMI sensing experiments, the prepared solution was diluted 17-fold with deionized water.

2.3 Detection of heavy metal ions in water

To evaluate the sensing performance of the prepared PEI–vanillin sensor solution, fluorescence emission studies were carried out in the presence of various HMIs. In a typical experiment, 2 mL of the PEI/vanillin solution was placed in a quartz cuvette, and different concentrations of target analytes were gradually introduced. For selectivity studies, the sensor was tested against eleven HMIs: Cu^{2+}, Cd^{2+}, Cr^{3+}, Co^{2+}, Fe^{3+}, Zn^{2+}, Mn^{2+}, Al^{3+}, Pb^{2+}, Hg^{2+}, and Ni^{2+}. The resulting mixtures were gently agitated and allowed to stabilize for a few minutes to ensure adequate interaction between the analytes and the sensing matrix. Fluorescence emission spectra were then recorded, and the fluorescence intensity at the characteristic emission wavelength was monitored to assess the selectivity and sensitivity of the sensor. Changes in fluorescence intensity, either enhancement or quenching, were used to evaluate the extent of interaction between each analyte and the PEI/vanillin system.

The efficiency of detection (η) was quantified using the equation[49]:

$$\eta = \frac{M_0 - M}{M_0} \times 100, \quad (1)$$

where M_0 denotes the fluorescence intensity of the blank PEI/vanillin solution, and M represents the fluorescence intensity after addition of the analyte. This calculation helps to determine the relative change in the intensity of the emission, reflecting the responsiveness of the sensor to each specific metal.

2.4 Characterization of the PEI–vanillin Schiff base system and its response to heavy metal ions

The synthesized polyethylenimine and vanillin-based Schiff base complexes were characterized using a series of spectroscopic and analytical techniques to confirm structural formation and their sensing behavior toward HMIs. UV-vis absorption spectra were recorded using a UV-Vis-NIR spectrophotometer (V-770, JASCO, Japan), capable of measuring in the wavelength range 190–2700 nm, to monitor changes in electronic transitions associated with imine bond formation. The vibrational properties were examined using a single reflection ATR-IR spectrophotometer (FT/IR-4X, JASCO, Japan) in the wavenumber range of 400–4000 cm^{-1}, which confirmed the formation of Schiff bases by examining the emergence of C═N stretching bands and distinctive peaks of functional groups in PEI and vanillin. To preliminarily evaluate the fluorescence behavior of the sensor material, the sample is observed under 450 nm filtered light using a solar simulator (SLB-300-A, Sciencetech Inc., Canada) powered by a xenon arc lamp and set to AM 1.5G–1 sun illumination. Fluorescence emission of the PEI–vanillin system and its response to HMIs is further examined using a spectrofluorometer (Jobin Yvon Fluorolog-3, Horiba, France). In addition, fluorescence lifetime measurements were carried out using time-correlated single photon counting (TCSPC) on a Fluorocube Lifetime System (Jobin-Yvon, Horiba, France), equipped with pulsed-diode excitation sources (LEDs: 280, 295, 340, 370, 390, and 460 nm), to assess the fluorescence lifespan and investigate the excited-state dynamics before and after metal ion contact. ^{1}H Nuclear magnetic resonance (NMR) spectra were recorded at 500 MHz (Bruker Avance III, Bruker, Germany) to confirm the formation of the Schiff base by identifying the characteristic imine proton signals and observing changes in the chemical shifts of PEI and vanillin after they were combined. X-ray photoelectron spectroscopy (XPS) measurements were carried out using a K-Alpha X-ray Photoelectron Spectrometer (Thermo Fisher Scientific, Waltham, USA) to investigate the changes in the surface chemical composition and binding environments of the PEI–vanillin probe before and after Cu^{2+} coordination.

3 Results and discussion

3.1 Structural confirmation

The formation of the PEI–vanillin Schiff base was confirmed by FTIR spectroscopy,[50,51] which provides evidence for the condensation reaction between the amine groups of PEI and the aldehyde functionality of vanillin. The reaction proceeds through a nucleophilic attack by the lone pair of electrons on the nitrogen atom of the primary amine groups in PEI, targeting the electrophilic carbon within the carbonyl group (C═O) of the aldehyde moiety in vanillin.[41] This leads to the formation of an imine (Schiff base; C═N) *via* a condensation reaction, with the release of a water molecule, as shown in Fig. 1.[52] The imine linkage serves as the core sensing motif, with the phenolic –OH and aromatic ring from vanillin potentially enhancing electron delocalization and metal-binding capacity.[24,53]

FTIR analysis revealed the disappearance of characteristic peaks corresponding to primary amine (–NH_2) and aldehyde (–CHO) groups, along with the appearance of a distinct stretching vibration near 1643 cm^{-1}, attributed to the imine (–C═N–) bond as shown in Fig. 2a. The emergence of the imine (C═N) stretching band at 1643 cm^{-1}, along with the disappearance of the aldehyde (C═O) peak at 1662 cm^{-1}, indicates successful Schiff base formation within the network.[45] As supporting evidence, the ^{1}H NMR spectrum in Fig. (2b) reveals a characteristic signal at 8 ppm after vanillin is added to PEI, attributable to the azomethine (–CH═N–) proton, thereby confirming Schiff base formation.[44] This signal, although relatively weak, which is typical due to low proton density and peak broadening in polymer-based systems, supports the successful condensation reaction between the amine groups of PEI and the aldehyde moieties of vanillin. The azomethine group, representing the imine (–C═N) linkage, plays a crucial role in the sensing functionality of the material. The FTIR spectrum of the PEI–vanillin film after Cu^{2+} coordination is provided in the SI

 This journal is © The Royal Society of Chemistry and the Centre National de la Recherche Scientifique 2026

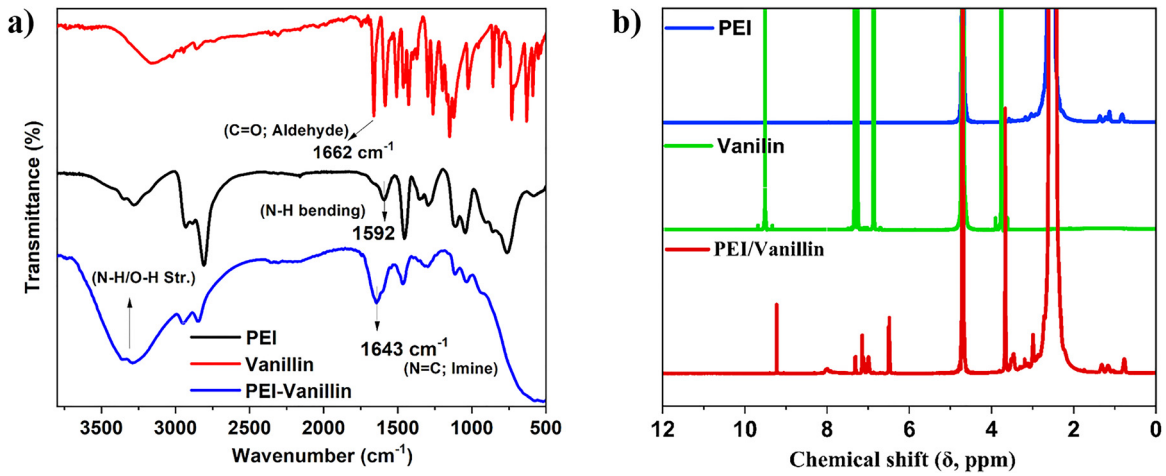


Fig. 2 (a) FTIR and (b) ^{1}H NMR spectra of PEI, vanillin, and PEI–vanillin.

(Fig. S3), and the observed spectral changes further support the proposed coordination mechanism.

3.2 Photophysical and fluorescence characteristics of PEI–vanillin

3.2.1 Absorption characteristics and band gap analysis of PEI/vanillin. Fig. 3a shows the UV-Vis absorption spectrum of the sensor material,[54,55] which exhibits a broad absorption band from 250–500 nm. Pristine PEI exhibited minimal absorbance throughout this range. Vanillin showed two characteristic absorption peaks at approximately 270 and 310 nm. Upon imine formation with PEI, a new bathochromically shifted peak appeared at ~360 nm in the UV-Vis spectrum of the PEI/vanillin system (Fig. 3a), which is attributed to the π–π* transition of the imine (–CH═N–) bonds.[56] This spectral shift confirms the successful formation of Schiff base linkages in the PEI–vanillin network.[57] The Tauc plot as shown in Fig. 3b reveals that the sensor material has an optical band gap of approximately 3.2 eV.

3.2.2 Excitation-dependent fluorescence and emission profile of PEI–vanillin. To assess the fluorescence behavior of the components, visual observations were carried out under 450 nm filtered light using a solar simulator. Visual observations under 450 nm filtered light using a solar simulator revealed a greenish-yellow emission as shown in Fig. S1a, indicating strong emissive behavior. This is further supported by the chromaticity diagram, which confirms emission in the yellow region as shown in Fig. S1b. Additionally, the 2D excitation–emission map demonstrates a broad fluorescence profile across the visible range, while the 3D surface plot illustrates the overall photoluminescence intensity distribution as shown in Fig. S1c and d, respectively, highlighting the robust emission characteristics of the system.

Excitation-dependent emission spectra recorded in the excitation range of 400–650 nm showed a broad emission spanning from ~500 to 550 nm, with a prominent emission peak observed around 550 nm. In particular, as shown in Fig. 4a excitation at 410 nm, corresponding to the maximum absorbance region, produced the strongest fluorescence response. Under this

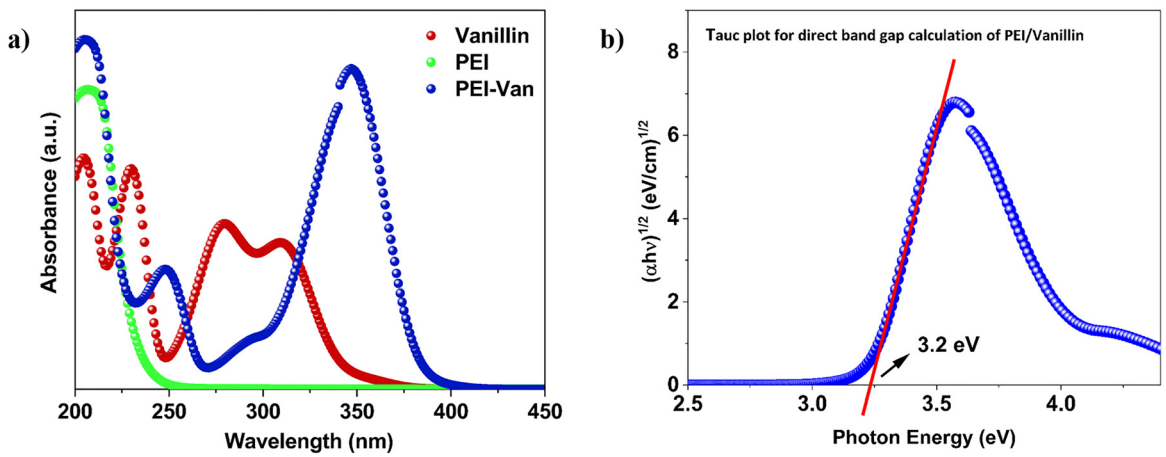


Fig. 3 (a) UV-Vis absorption spectra of pristine PEI, vanillin, and the synthesized PEI–vanillin conjugate. The bathochromically shifted absorption band at ~360 nm in the PEI–vanillin system indicates Schiff-base (–CH═N–) formation and enhanced π-conjugation. (b) Tauc plot of the PEI–vanillin system derived from UV-Vis data, indicating an optical bandgap of approximately 3.2 eV.

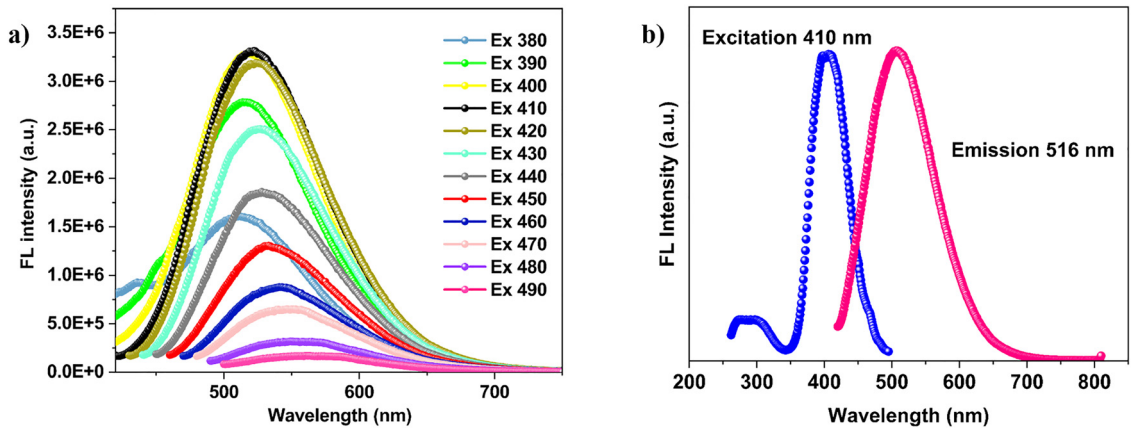


Fig. 4 (a) Excitation-dependent fluorescence emission spectra of the PEI–vanillin system recorded across excitation wavelengths from 380 to 490 nm. A broad emission band spanning 400–650 nm is observed, indicating strong visible-range fluorescence. (b) Fluorescence excitation and emission spectra of the PEI–vanillin system at the optimized excitation wavelength of 410 nm, showing a maximum emission peak at 516 nm.

condition, a distinct emission peak appeared at ~516 nm, as shown in Fig. 4b. Additionally, the image in Fig. S1a shows a visible greenish-yellow fluorescence observable to the naked eye, confirming effective emission in the visible range. This greenish-yellow fluorescence is attributed to the formation of –CH═N– linkages and enhanced π-conjugation within the PEI–vanillin network, which promote efficient fluorescence, consistent with previous reports on imine-linked π-conjugated polymer networks exhibiting visible-light activity.[58] Also it should be noted that, although vanillin and PEI exhibit negligible fluorescence, the formation of the PEI–vanillin Schiff base network induces a significant fluorescence response, which can be attributed to the formation of the imine linkage and the constrained polymeric environment that limits molecular motion (as shown in Fig. S2).

3.2.3 pH responsiveness and long-term photostability of the PEI–vanillin sensor. The photophysical characteristics of the PEI–vanillin system, including its fluorescence emission, chromaticity coordinates, and excitation–emission behavior, are provided in the SI (Fig. S1). The photophysical stability of the PEI–vanillin sensor under changing pH settings was examined using fluorescence emission spectra (λ_{ex} = 410 nm). The sensor material was subjected to fast pH variations over a wide range (pH 1–12) using HCl and NaOH to replicate acidic and basic conditions. As shown in Fig. 5a the fluorescence intensity of the PEI–vanillin system remained stable across a wide pH range (pH 4–12), with the highest emission observed at neutral pH (~7, DI water). A marked decrease in fluorescence occurred under strongly acidic conditions (pH 1–3), likely due to protonation of imine linkages disrupting the conjugated structure.[59] In general, the luminescent properties of Schiff base molecules are largely influenced by protonation and deprotonation processes at specific sites within the molecule.[60] Schiff bases typically remain stable in aqueous solutions and can reversibly switch between protonated and deprotonated forms depending on pH.[61] As shown in Fig. 5a, at higher pH values (pH 7–12), the system maintained its emission, suggesting that imine bonds remain stable in alkaline environments. They tend to degrade under strongly acidic conditions (pH < 3) due to protonation of the imine bond. Furthermore, the actual pH of the sensing system was monitored before and after Cu^{2+} addition to evaluate any possible pH variation during the detection process. The pristine PEI–vanillin solution exhibited a pH of 7.5, while the pH after Cu^{2+} addition was found to be 7.3. The negligible change in pH indicates that the fluorescence quenching observed upon Cu^{2+} addition is not primarily induced by pH variation but is associated with the coordination interaction between Cu^{2+} ions and the nitrogen/oxygen donor sites of the PEI–vanillin network.

To evaluate the photostability of the PEI–vanillin system over extended storage, fluorescence emission was monitored periodically for over six months under ambient temperature conditions, with the samples stored in the dark (wrapped in aluminum foil). The progressive increase in fluorescence intensity over the first few days (as shown in Fig. 5b) is most likely caused by the dynamic nature of the imine bonds in the PEI–vanillin network,[62,63] which continue to reorganize and stabilize after initial synthesis. The observed rise in fluorescence intensity over the aging period (up to 8 days) is likely due to the progressive restriction of intramolecular motions and the formation of a more rigid polymer environment. Consistent with this evolution, the sensor solution also exhibits a gradual visual color change from pale yellow to deep brownish-yellow (Fig. 5c), indicating increased conjugation and electronic delocalization within the PEI–vanillin network as imine linkages continue to form and reorganize. This behavior is well aligned with aggregation-induced emission (AIE) in polymeric systems, where increasing structural rigidity and aggregation constrain molecular motion and lead to enhanced fluorescence.[64] Once the polymer network reaches a stable configuration, both the color and fluorescence intensity remain unchanged over prolonged storage.

3.3 Fluorescence quenching response: metal-induced quenching behavior of the PEI–vanillin sensor system

To explore the sensing capability of the PEI–vanillin system towards various HMIs, both visual and fluorescence responses were systematically examined. As shown in Fig. 6a, the addition

 This journal is © The Royal Society of Chemistry and the Centre National de la Recherche Scientifique 2026

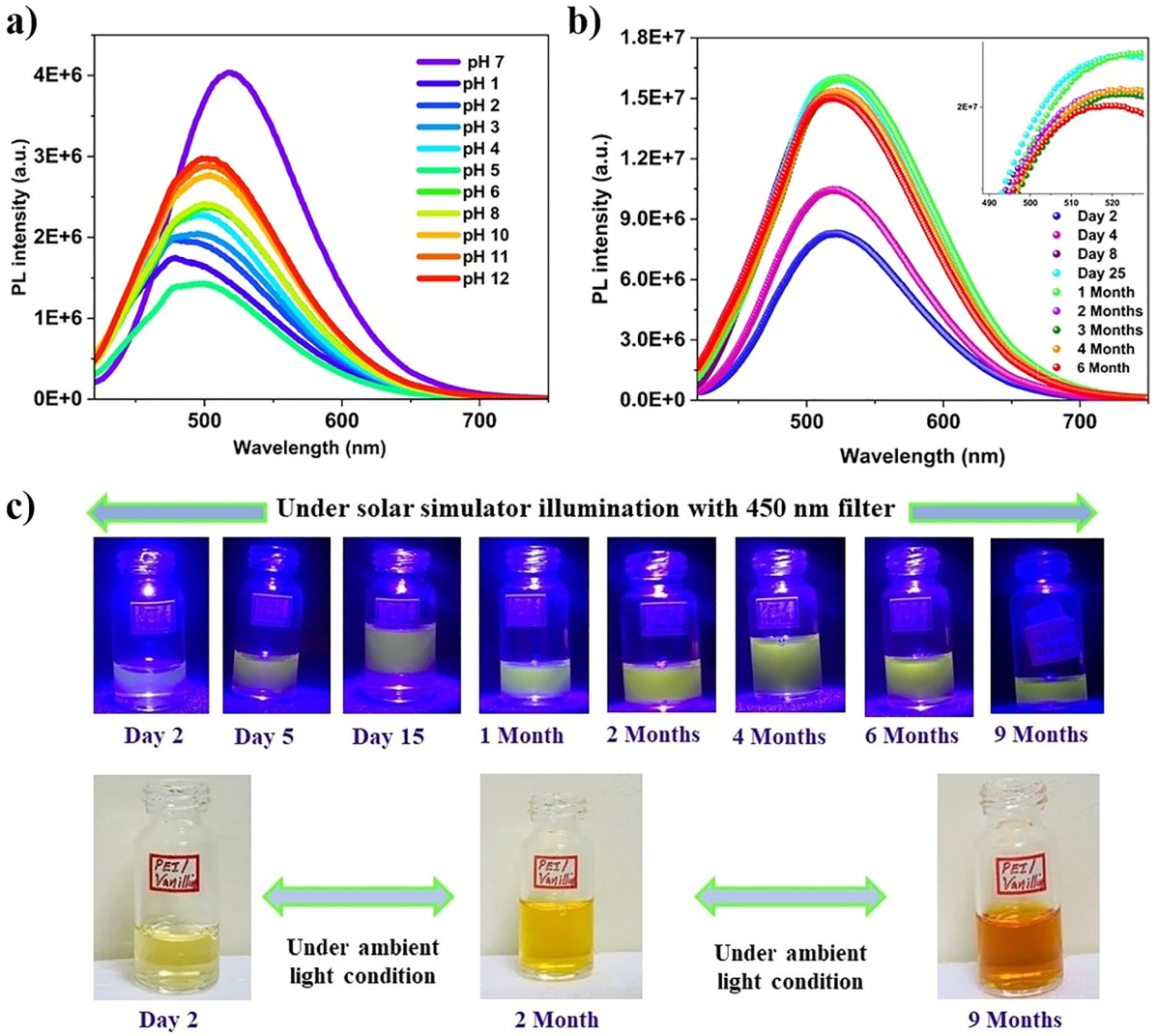


Fig. 5 (a) Fluorescence emission spectra of the PEI–vanillin sensor recorded under varying pH conditions, demonstrating its pH-responsive behavior. (b) Long-term photostability assessment of the PEI–vanillin system (at pH 7) over a six-month period, with fluorescence spectra recorded at periodic intervals under ambient conditions. (c) Time-dependent behavior of the PEI–vanillin system under simulated solar irradiation ($\lambda > 450$ nm), demonstrating stable fluorescence with no observable color change, whereas under natural light, the solution undergoes a gradual transition from pale yellow to deep brownish-yellow over extended periods.

of 10 mM metal ion solutions to the PEI–vanillin sensor revealed distinct responses depending on the ion. Visually, only Cu induced a pronounced greenish-blue coloration, suggesting strong complexation or redox-driven changes. Under 450 nm excitation using a solar simulator, Cu^{2+} led to significant fluorescence quenching (Fig. 6b). Interestingly, Fe^{3+} ions also induced fluorescence quenching, but instead of simply dimming the signal, the emission color shifted to pink (Fig. 6c), suggesting a unique interaction or altered emission pathway. In contrast, Co induced only slight quenching (Fig. 6d), demonstrating comparatively weaker interaction.

To further evaluate the sensing performance of the PEI–vanillin system, fluorescence responses were recorded against a range of HMIs (Fig. 7a). Among the ions tested, Cu^{2+} induced the most significant quenching of the emission intensity, while Co^{2+} and Fe^{3+} showed moderate effects and Ni^{2+} caused only slight changes. Other ions produced negligible influence, confirming the selectivity of the sensor. The time-dependent study with Cu^{2+} (Fig. 7b) revealed an immediate and pronounced quenching of the emission signal, with a marginal further decrease observed within the first 2 minutes. Thereafter, the fluorescence intensity remained essentially unchanged across the measured intervals up to 45 minutes. This trend indicates that the interaction between Cu^{2+} and the PEI–vanillin system is both rapid and stable, underscoring the importance of defining a consistent contact time when assessing the sensor response towards other HMIs.

To quantitatively evaluate the fluorescence quenching efficiency of the PEI–vanillin sensor system, fluorescence spectra were recorded across three concentration regimes, millimolar (mM), micromolar (μM), and nanomolar (nM), for Cu^{2+}. Copper concentration varies significantly depending on the source,

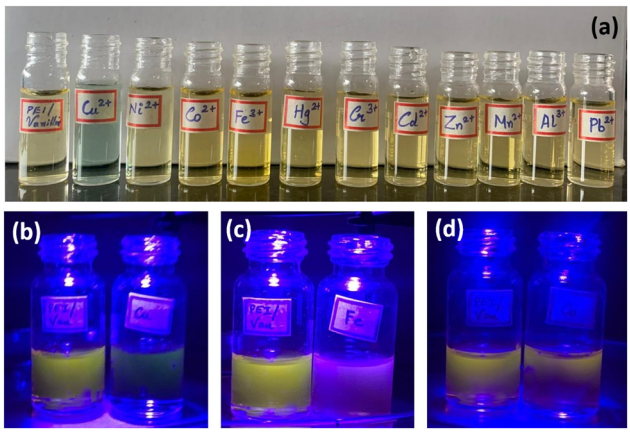


Fig. 6 (a) Visual color change of PEI–vanillin aqueous solution after adding 10 mM of various heavy metal ion salts; only Cu^{2+} produces a noticeable blue coloration. Fluorescence response under a solar simulator with a 450 nm filter shows (b) strong quenching with Cu^{2+}, (c) pink fluorescence observed with Fe^{3+}, indicating selective emission behavior, and (d) slight quenching with Co^{2+}.

reflecting differences in the degree of anthropogenic and natural contamination. Industrial effluents such as electroplating and mining wastewater exhibit relatively high Cu^{2+} levels (0.5–1000 mM range), whereas environmental and biological samples like municipal wastewater, surface water, and drinking water typically contain much lower concentrations (μM to nM range).[65] This wide concentration range highlights the importance of developing sensors capable of detecting Cu^{2+} across both high (mM) and trace (μM–nM) levels.

As Cu^{2+} displayed pronounced and progressive quenching over the entire range, measurements were extended down to the 10 nM concentration level to establish the full dynamic response. Since Co^{2+}, Ni^{2+}, and Fe^{3+} also exhibited noticeable quenching effects, as evident from the comparative fluorescence response, Fig. 7a, their spectra were likewise recorded. However, for these ions, the quenching trend reached saturation around 1 mM concentration, and therefore further dilution into the lower concentration ranges was not pursued. As shown in Fig. 8a, a gradual decrease in fluorescence intensity with increasing Cu^{2+} concentration confirmed the effective quenching behavior of the system over a broad dynamic range. The corresponding fluorescence intensity values plotted against Cu^{2+} concentration with error bars (n = 3) are presented in Fig. 8b, demonstrating reproducibility, sensitivity, and a well-defined linear response across all regimes. This linearity highlights the potential of the PEI–vanillin system for the quantitative detection of unknown Cu^{2+} concentrations in aqueous samples.

In contrast, the quenching responses observed for Fe^{3+}, Co^{2+}, and Ni^{2+} were less consistent. For Co^{2+} as shown in Fig. 8c, a moderate quenching effect with some degree of linearity was observed in the higher concentration range (10 mM to 1 mM); however, at micromolar levels, the fluorescence intensity values remained nearly unchanged, indicating poor sensitivity and no clear linear trend, as shown in Fig. 8c and d. A similar pattern was observed for Fe^{3+} (as shown in Fig. 8e and f), where initial quenching occurred at 10–1 mM concentrations but plateaued quickly, showing negligible changes at lower concentrations. The response for Ni^{2+} was especially weak and erratic across the tested regimes (as shown in Fig. S6). Thus, while the sensor demonstrated strong and selective fluorescence quenching toward Cu^{2+}, its responses to Fe^{3+}, Co^{2+}, and Ni^{2+} were weak, inconsistent, and non-linear, underscoring its limited applicability for these ions.

3.4 Investigation of Cu^{2+} induced fluorescence quenching

To investigate the interaction between PEI–vanillin and Cu^{2+} ions, UV-Vis absorption experiments were carried out by gradually increasing the concentration of Cu^{2+}. As shown in Figure S8, the characteristic absorption band of PEI–vanillin centered at approximately 350 nm gradually decreased in intensity with increasing Cu^{2+} concentration, while no significant shift in the absorption maximum was observed.[66] The decrease in absorbance indicates the interaction of Cu^{2+} ions with the Schiff base moieties of PEI–vanillin through coordination with the imine nitrogen and phenolic oxygen atoms. The absence of an appreciable wavelength shift suggests that Cu^{2+} binding does not

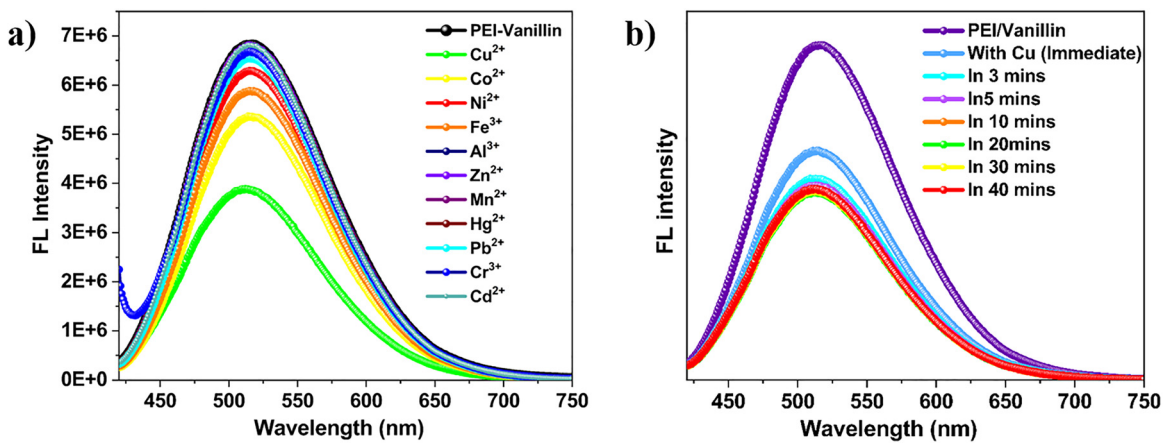


Fig. 7 (a) Fluorescence responses of the PEI–vanillin sensor towards different heavy metal ions. (b) Time-dependent fluorescence quenching of Cu^{2+}.

 This journal is © The Royal Society of Chemistry and the Centre National de la Recherche Scientifique 2026

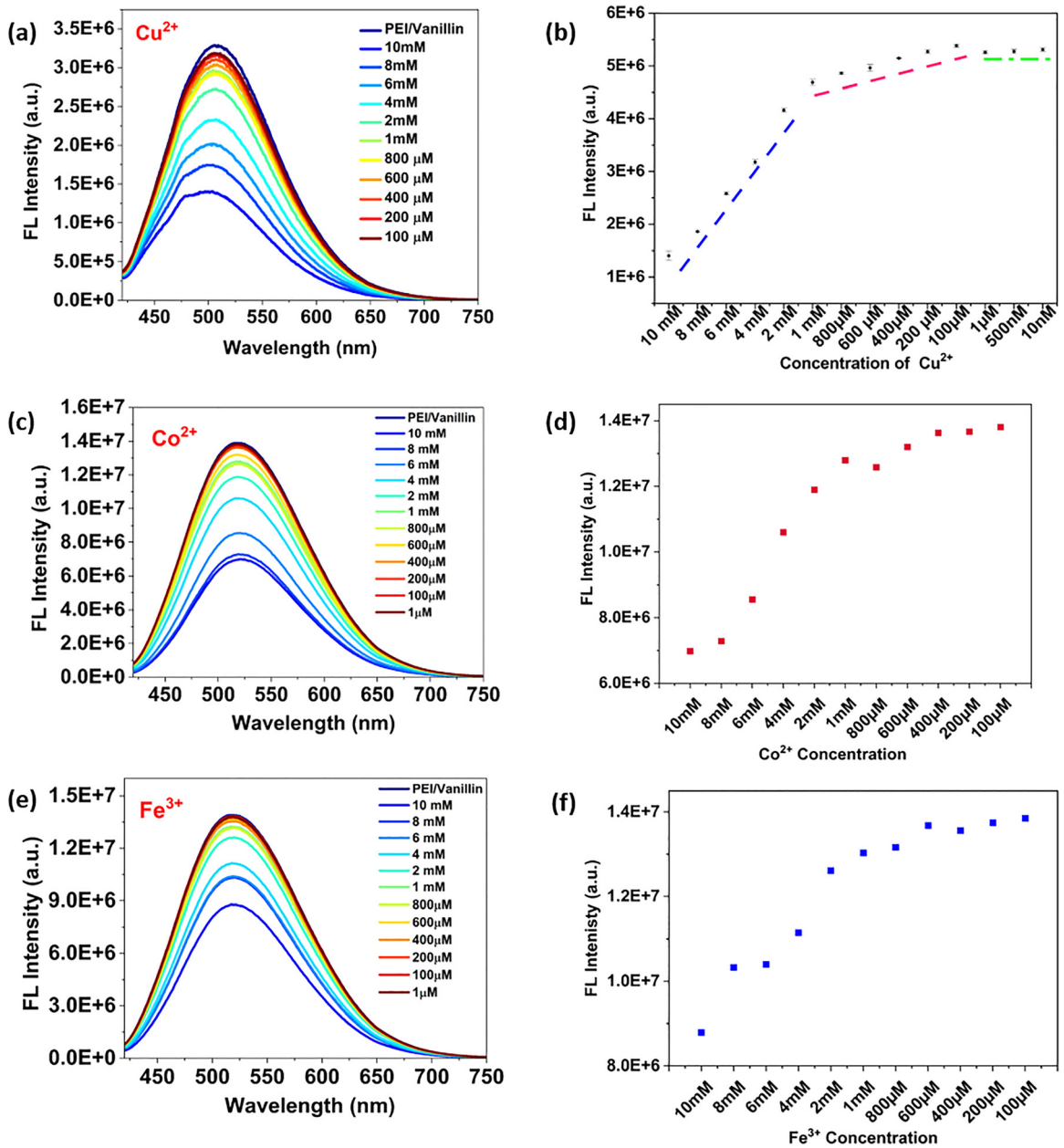


Fig. 8 Fluorescence quenching of the PEI–vanillin sensor system with (a) Cu^{2+} across the mM, µM, and nM regimes, showing progressive quenching and (b) the corresponding calibration plot with error bars (n = 3); (c) Co^{2+} and (e) Fe^{3+}, showing concentration-dependent quenching with their respective linearity plots (d and f).

substantially alter the electronic structure of the chromophore but instead favors the formation of a coordination complex in the ground state.[67]

To further verify the coordination of Cu^{2+} with the PEI/vanillin network, XPS analysis was also performed before and after Cu^{2+} addition, as shown in Fig. S4 and S5. The XPS survey spectrum of the Cu^{2+}-treated sample (Fig. S4) exhibits the characteristic Cu 2p signal (approximately 930–955 eV), which is absent in the pristine PEI/vanillin film, confirming the successful incorporation of Cu^{2+} into the polymer matrix.[36,68,69] In addition, the survey and high-resolution spectra show noticeable changes in the chemical environments of the C, N, and O atoms following Cu^{2+} binding, indicating interactions between the metal ions and the functional groups present in the PEI/vanillin framework. These observations, together with the FTIR results (as illustrated in Fig. S2), provide strong evidence for the formation of a PEI/vanillin–Cu^{2+} coordination complex responsible for the fluorescence sensing behavior.

Fig. S5 presents the high-resolution C1s, N1s, and O1s XPS spectra of the PEI/vanillin film before and after Cu^{2+} addition. Following Cu^{2+} coordination, subtle changes in the peak positions and line shapes of the C1s, N1s, and O1s spectra are observed, reflecting modifications in the local chemical environments of carbon-, nitrogen-, and oxygen-containing functional

groups. The most noticeable changes occur in the N1s and O1s spectra, suggesting the involvement of amine/imine nitrogen and oxygen-containing groups in Cu^{2+} coordination. These spectral variations, together with the FTIR results, provide strong evidence for the formation of a PEI/vanillin–Cu^{2+} coordination complex. The fluorescence quenching behavior of PEI–vanillin toward Cu^{2+} was further evaluated using the Stern–Volmer relationship[70]:

$$\frac{F_0}{F} = 1 + K_{SV}[Q] \quad (2)$$

where F_0 is the fluorescence intensity in the absence of the quencher, F is the fluorescence intensity in the presence of the quencher, K_{SV} is the Stern–Volmer quenching constant, and [Q] is the concentration of the quencher (Cu^{2+}).

A linear Stern–Volmer plot was obtained in the concentration range of 100–1000 μM (as shown in Fig. S9), following the equation,

$$\frac{F_0}{F} = 0.99274 + 1.57513 \times 10^{-4}[Cu^{2+}] \quad (3)$$

with a correlation coefficient (R^2) of 0.98449. The calculated Stern–Volmer quenching constant (K_{SV}) was 157.5 M^{-1}, indicating efficient interaction between Cu^{2+} ions and the PEI–vanillin fluorescent network. The observed linear relationship suggests that the quenching process proceeds predominantly through a single quenching mechanism within the investigated concentration range.

Furthermore, the fluorescence lifetime measurements revealed a slight decrease in the average lifetime of PEI–vanillin after Cu^{2+} addition, suggesting changes in the excited-state dynamics of the probe upon Cu^{2+} interaction. The detailed lifetime analysis and its implications for the quenching mechanism are discussed in the following section. When considered together with the UV-Vis absorption, XPS characterization, and Stern–Volmer analysis, these results demonstrate that Cu^{2+} forms a coordination complex with the imine nitrogen and phenolic oxygen atoms of PEI–vanillin. The resulting coordination-induced structural changes facilitate non-radiative deactivation, leading to efficient fluorescence quenching.

3.5 TCSPC-based lifetime analysis, deconvoluted PL spectrum and band structure evaluation

To gain deeper insight into the fluorescence behavior of the PEI/vanillin-based system, time-correlated single-photon counting (TCSPC) was employed to measure the fluorescence lifetime. This technique is highly sensitive and well-suited for capturing fluorescence decay profiles on the picosecond to nanosecond timescale. The average lifetime of the system was determined by fitting the decay profile to a multi-exponential model. The corresponding fluorescence decay can be expressed as:

$$I(t) = B_1 e^{-t/\tau_1} + B_2 e^{-t/\tau_2} + B_3 e^{-t/\tau_3} \quad (4)$$

where $I(t)$ is the fluorescence intensity at time t, and the component lifetimes (τ_1, τ_2, τ_3) and their corresponding pre-exponential factors (B_1, B_2, B_3).

Then, the mean lifetime (τ_0) is calculated as:

$$\tau_0 = \frac{B_1\tau_1^2 + B_2\tau_2^2 + B_3\tau_3^2}{B_1\tau_1 + B_2\tau_2 + B_3\tau_3} \quad (5)$$

Fig. S10–S12 show the time-resolved fluorescence decay profiles of PEI–vanillin in the absence and presence of Cu^{2+}, respectively. From the decay curve, the calculated mean lifetime is 4.17 ns, which supports the radiative recombination process responsible for the observed fluorescence[49] of the PEI–vanillin system. In both cases, the decay follows a multiexponential behavior, indicating the presence of multiple emissive sites in the system. From Table S1, it is evident that in the presence of HMI Cu^{2+}, the fluorescence lifetime decreases marginally (from 4.17 ns to 3.788 ns), suggesting the involvement of additional non-radiative decay pathways,[71] thereby leading to fluorescence quenching. The χ^2 value (1.5) indicates that the decay curve is well fitted.

The fluorescence spectrum was subjected to Gaussian fitting deconvolution (as illustrated in Fig. 9a) to better understand the emission mechanism. The resulting emission peaks at 2.80,

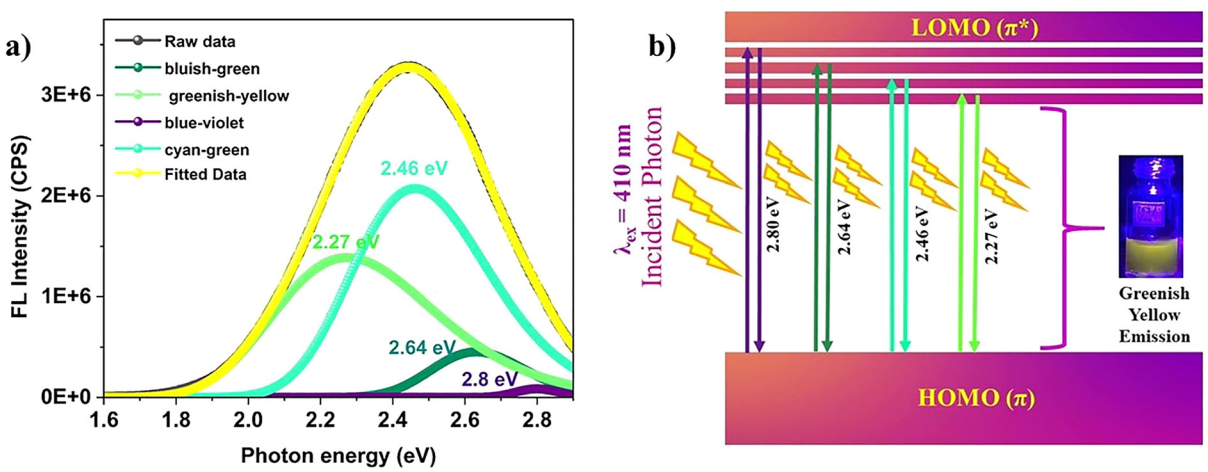


Fig. 9 (a) Deconvoluted photoluminescence spectra and (b) bandgap alignment.

 This journal is © The Royal Society of Chemistry and the Centre National de la Recherche Scientifique 2026

2.64, 2.46, and 2.27 eV indicate the presence of multiple emissive states, each arising from distinct radiative recombination pathways within the Schiff base-functionalized polymer matrix (C–N derived π–π* and n–π* transitions or aggregation effects or exciplex formation).[24,56,72] The higher energy emission peak at 2.80 eV may be associated with π–π* transitions localized within the imine (C═N) moiety, which serves as the primary fluorophore in the system. The subsequent peak at 2.64 eV likely arises from n–π* transitions, possibly involving lone pair electrons on nitrogen atoms of the PEI chain interacting with the conjugated system. The lower energy peaks at 2.46 eV and 2.27 eV can be attributed to localized states influenced by hydrogen bonding, molecular aggregation, or the formation of weakly emissive exciplexes within the polymeric framework. The presence of multiple emissive states highlights the heterogeneous nature of the PEI/vanillin composite. This multi-channel emission process, as depicted in the energy alignment diagram (Fig. 9b), involves electronic transitions from the HOMO to different LUMO-adjacent states influenced by structural and chemical heterogeneity. The superposition of these emissions results in the observed greenish-yellow fluorescence, making the system suitable for optical sensing applications.

3.6 Fluorescence-based sensitivity profiling of the PEI–vanillin sensor against different metal ions

Fluorescence quenching experiments performed at an analyte concentration of 10 mM show a clear and selective response toward Cu^{2+} as shown in Fig. 10. Cu produced a 43.17% decrease in emission intensity, whereas Co^{2+}, Fe^{3+}, Ni^{2+} and the remaining tested ions produced substantially lower effects (Co 21.21%, Fe 13.57%, Ni 7.63%, Pb 3.92%, Mn 2.80%, Cr 1.79%, Al 1.16%, Hg 0.82%, Zn 0.01%, Cd −0.004%). These results indicate that Cu is the dominant quencher under the conditions tested, with Co and Fe as the only moderately interfering species. Importantly, we verified that at substantially lower analyte concentrations, the responses of non-target ions diminish to negligible levels and the sensor's Cu selectivity improves markedly.

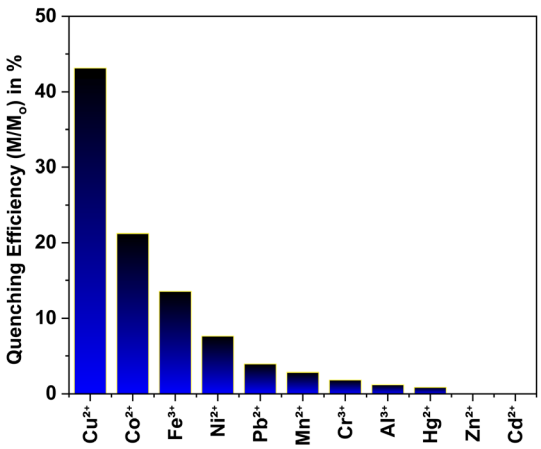


Fig. 10 Fluorescence quenching (%) of the sensor toward different metal ions (10 mM), showing strong selectivity for Cu^{2+}.

The selectivity of the PEI–vanillin sensor system toward Cu^{2+} was further tested using a fluorescence-based interference study, which was conducted using ten different HMIs. Fluorescence measurements were first recorded for Cu^{2+} alone at a concentration of 10 mM, followed by measurements of Cu^{2+} in the presence of each HMI at the same concentration. As shown in the bar graph (Fig. 11a), most of the tested HMIs caused minimal interference with Cu^{2+} induced quenching. However, Co^{2+}, Ni^{2+}, and Fe^{3+} showed a modest reduction in quenching efficiency, indicating potential interference at a higher concentration range. To further evaluate this, a second set of measurements was conducted at a lower concentration (600 μM), focusing only on these three ions. At this concentration level, interference from Co^{2+}, Ni^{2+}, and Fe^{3+} was found to be negligible (as shown in Fig. 11b), confirming the sensor's reliable selectivity for Cu^{2+} in lower concentration regimes.

As summarized in Table 1, while several reported sensors offer ultra-low nanomolar detection limits for trace-level analysis, the WHO guideline for Cu^{2+} in drinking water is about 2 μM.[65] In this context, the PEI–vanillin polymer sensor remains highly relevant, as its detection capability adequately aligns with regulatory thresholds while ensuring reliable monitoring. Additionally, as highlighted in the table, it offers key advantages such as a fully aqueous system, the absence of toxic materials, low cost, and simple synthesis. These features make it a practical and sustainable platform for real-time and field-deployable copper ion detection.

3.7 Future directions: immobilization of PEI–vanillin on Whatman filter paper for Cu^{2+} sensing

To demonstrate the feasibility of portable sensing as a proof-of-concept, the PEI–vanillin probe was immobilized onto WFP. The excitation–emission behavior was examined by exciting the sensor system from 340 to 490 nm in steps of 20 nm. The strongest emission was obtained at 470 nm excitation (Fig. 12a), which was used for subsequent measurements. In solution, the PEI–vanillin fluorophore is well-dispersed, which allows a maximum excitation at 410 nm, as was found in Fig. 4b. However, when coated and dried on WFP, the molecular environment changes: fluorophores become immobilized or may have aggregated and interacted with the cellulose matrix, altering the local polarity and molecular motion. Such transitions often lead to red-shifted excitation,[81] which explains why the maximum

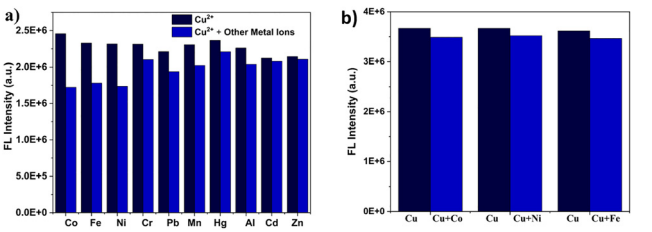


Fig. 11 Fluorescence interference study of the PEI–vanillin sensor system toward Cu^{2+}: (a) comparative fluorescence response at 10 mM concentration of Cu^{2+} with different HMIs, (b) fluorescence response at a lower concentration (600 μM) of Cu^{2+} with Co^{2+}, Ni^{2+}, and Fe^{3+}.

Table 1 Comparative evaluation of reported Cu^{2+} sensors based on detection limits and practical applicability

Sensor/probe	Medium	LOD	Remarks (material + practical insight)	Ref.
Rhodamine–CdTe QD hybrid	Ethanol/water	8.4 nM	Although the sensing medium is a relatively mild ethanol–water mixture, the use of cadmium-based quantum dots introduces significant toxicity concerns, limiting environmental friendliness and sustainability	73
Cytidine-stabilized Cu nanoclusters	Water + citrate buffer	0.032 μM	Biomolecule-stabilized, relatively biocompatible. However, reliance on metal nanoclusters may raise concerns regarding metal-associated toxicity and environmental impact	74
Spiropyran-based sensor	Ethanol/PVC membrane	0.15 μM	Uses organic solvent and polymer membrane; not fully aqueous and involves synthetic dye components	75
Optical fiber SiQD sensor	Aqueous buffer (BR buffer)/hydrogel	3.58 nM	Aqueous system but relies on a nanomaterial-based probe and optical fiber setup, making it instrument-dependent and less convenient for routine applications	76
Lysozyme–Au nanoclusters	Water-based system	~9 nM	Green synthesis (protein-based), but relies on gold nanoclusters (metal-based probe)	77
BODIPY dye sensor	Acetonitrile/water	1.28 μM	Uses organic solvent and synthetic dye; not fully aqueous and requires an organic medium for sensing	78
Carbazole-based fluorescent probe	DMSO–H_2O mixed solvent	11.9 nM	Organic–aqueous medium required, limiting full water compatibility despite good sensitivity and selectivity	79
CdSe/ZnS QD optical fiber sensor	PEGDA hydrogel/water	0.8 nM	Ultra-sensitive and fast optical fiber sensor, but uses CdSe/ZnS QDs (toxic heavy-metal nanomaterial), limiting sustainability and environmental safety	80
PEI–vanillin based	Water	290 nM	The sensing system is based on an aqueous medium and avoids the use of heavy metal components. Although PEI exhibits dose-dependent cytotoxicity, the low concentration employed minimizes environmental and biological risks compared to nanomaterial- or synthetic probe-based systems	This work

excitation shifted from 410 nm in solution to 470 nm when immobilized on WFP. For instance, phosphorus-doped carbon dots exhibit a tunable emission red-shift with an increase in concentration, from 455 to 595 nm by virtue of a phenomenon termed aggregation-induced red shift emission (AIRSE).[82]

The identified excitation wavelength of 470 nm was then applied to study Cu^{2+} interactions on the PEI/vanillin-coated WFP surface. The addition of 1 mM Cu^{2+} ions induced a clear fluorescence quenching response (Fig. 12b), demonstrating the selective sensing capability of the PEI/vanillin–WFP composite. In addition to the fluorescence response, a distinct bluish-green coloration was visually observed on the PEI/vanillin-coated WFP upon exposure to Cu^{2+}, as shown in Fig. 12c. This observable color change enables rapid, naked-eye detection without the need for sophisticated instrumentation. The fluorescence emission spectra of the PEI–vanillin coated WFP sensor recorded on Day 2 and Day 10 are shown in Fig. S14. The spectra demonstrate that the fluorescence response was retained during storage, with only a slight shift in the emission maximum and no significant loss in fluorescence intensity. Since the PEI–vanillin probe exhibits excellent long-term stability in the liquid state (up to nine months), these preliminary results provide a promising foundation for future optimization of the paper-based sensor with respect to repeatability, response time, and extended storage stability. These results also highlight the potential for adapting the aqueous PEI–vanillin system into disposable paper-strip sensors, with future opportunities for integration into simple portable readout platforms, such as smartphone-assisted detection, for practical point-of-use water quality monitoring.

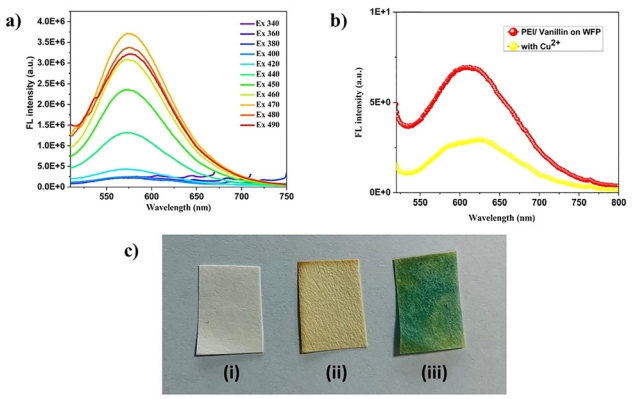


Fig. 12 (a) Fluorescence excitation–emission spectra of PV in aqueous solution recorded at excitation wavelengths from 340 to 490 nm (20 nm intervals), showing maximum emission intensity at 470 nm excitation. (b) Fluorescence emission spectra of PV-coated Whatman filter paper in the absence and presence of Cu^{2+} ions (1 mM). (c) Comparison of pristine Whatman filter paper (i), PV-coated paper (ii), and the same after Cu^{2+} (10 mM) treatment, showing the distinct bluish-green coloration upon complexation (iii).

4. Conclusion

Unlike many previously reported PEI-based fluorescent sensors that rely on synthetic aldehydes, multistep surface functionalization, or complex immobilization strategies, the present sensing platform was successfully fabricated through a simple one-pot aqueous Schiff base reaction between PEI and the naturally derived aldehyde vanillin, without requiring additional chemical modification or hazardous reagents. The resulting PEI–vanillin fluorescent probe exhibited efficient and selective fluorescence quenching toward Cu^{2+} ions in aqueous media over a broad concentration range, with a low limit of detection of approximately 290 nM.

Mechanistic investigations using UV-Vis absorption, X-ray photoelectron spectroscopy (XPS), Stern–Volmer analysis, and fluorescence lifetime measurements collectively revealed that

 This journal is © The Royal Society of Chemistry and the Centre National de la Recherche Scientifique 2026

Cu^{2+} ions coordinate with the imine nitrogen and phenolic oxygen atoms of the PEI–vanillin network. The resulting coordination-induced complex formation promotes non-radiative relaxation pathways, leading to efficient fluorescence quenching. The sensor also demonstrated excellent selectivity toward Cu^{2+}. Interference studies using ten common HMIs confirmed negligible overlap at low concentrations (micromolar level of 600 μM) and only modest overlaps for Co^{2+}, Ni^{2+}, and Fe^{3+} at elevated concentration (10 mM), affirming high selectivity for Cu^{2+}.

The aqueous compatibility, environmentally benign synthesis, and reproducible sensing performance highlight the practical advantages of the proposed platform over conventional PEI-based fluorescent sensors. Furthermore, the successful proof-of-concept demonstration on Whatman filter paper suggests the feasibility of developing portable and low-cost paper-based sensing devices for rapid on-site Cu^{2+} detection.

Author contributions

Berly Robert: conceptualization, investigation, methodology, visualization, data curation, validation, and writing – original draft. **Mohanraj Jagannathan**: data curation, visualization, and validation. **Moon Il Kim**: visualization and validation. **Sreeram K. Kalpathy**: validation, visualization, supervision, project administration, and writing: review & editing.

Conflicts of interest

There are no conflicts to declare.

Data availability

The data supporting the findings of this study are available within the article and its supplementary information (SI). Supplementary information is available. See DOI: https://doi.org/10.1039/d6nj02037b.

Acknowledgements

The authors acknowledge funding from the following sources for research: (1) National Post-Doctoral Fellowship from the Anusandhan National Research Foundation (ANRF), Department of Science and Technology, Government of India (File Number: PDF/2023/002437), (2) Ministry of Education, Government of India through the Swachhta Action Plan (SAP) scheme (Grant number SAP22-IITM-056), (3) HSBC India through the Center for Resource Efficiency, Recyclability, and Circularity in Energy Transition, School of Sustainability, IIT Madras (Grant No: CR24251368CHHSBC008836), and they thank the SAIF facility, IIT Madras, for providing instrumental support.

References

1 B. Robert, S. S. Kumar, T. Thomas and S. K. Kalpathy, Can recycled e-waste polymers power the future of sensors?, *J. Mater. Chem. A*, 2026, **14**, 13318–13331.
2 S. S. Kumar, B. Robert, S. K. Kalpathy and T. Thomas, Polymeric sensors at the crossroads of sustainability and scalability: low-temperature fabrication for environmental and health monitoring, *RSC Appl. Polym.*, 2026, **4**, 861–891.
3 N. H. Ab Hamid, M. I. H. bin Mohd Tahir, A. Chowdhury, A. H. Nordin, A. A. Alshaikh, M. A. Suid, N. azaruddin, N. D. Nozaizeli, S. Sharma and A. I. Rushdan, The current state-of-art of copper removal from wastewater: A review, *Water*, 2022, **14**, 3086.
4 C. E. Ugwu, A. M. Igbokwe, S. M. Suru, C. C. Dike, A. N. Mbachu and H. C. C. Maduka, Evaluating the human health risks of heavy metal contamination in copper and steel factory effluents in Nnewi, Anambra State, Nigeria, *Toxicol. Rep.*, 2024, **12**, 614–621.
5 E. I. Solomon, D. E. Heppner, E. M. Johnston, J. W. Ginsbach, J. Cirera, M. Qayyum, M. T. Kieber-Emmons, C. H. Kjaergaard, R. G. Hadt and L. Tian, Copper active sites in biology, *Chem. Rev.*, 2014, **114**, 3659–3853.
6 L. M. Gaetke and C. K. Chow, Copper toxicity, oxidative stress, and antioxidant nutrients, *Toxicology*, 2003, **189**, 147–163.
7 R. Manne, M. M. R. M. Kumaradoss, R. S. R. Iska, A. Devarajan and N. Mekala, Water quality and risk assessment of copper content in drinking water stored in copper container, *Appl. Water Sci.*, 2022, **12**, 27.
8 H. Zhang, Q. Zhang, X. Ji, B. Han, J. Wang and C. Han, Portable Bacterial Cellulose-Based Fluorescent Sensor for Rapid and Sensitive Detection of Copper in Food and Environmental Samples, *Molecules*, 2025, **30**, 3633.
9 R. V. Timoshenko, P. V. Gorelkin, A. N. Vaneev, O. O. Krasnovskaya, R. A. Akasov, A. S. Garanina, D. A. Khochenkov, T. M. Iakimova, N. L. Klyachko and T. O. Abakumova, *et al.*, Electrochemical nanopipette sensor for in vitro/in vivo detection of Cu^{2+} ions, *Anal. Chem.*, 2023, **96**, 127–136.
10 J. Sun, B. Bresson, E. Martwong, P. Nuchanong, G. Lefèvre, D. Mercier, Y. Tran, S. Griveau and C. Slim, Portable Copper(II) Sensor with High Sensitivity Based on Hydrogel Modified Screen-printed Carbon Electrode applicable to seawater and drinking water analysis, *Sens. Actuators, B*, 2026, 139419.
11 B. Robert and S. K. Kalpathy, Future prospects, challenges and opportunities in detecting heavy metal ions in water, *J. Water Process Eng.*, 2025, **75**, 107992.
12 S. Lai, Y. Jin, L. Shi, R. Zhou and Y. Li, Fluorescence sensing mechanisms of versatile graphene quantum dots toward commonly encountered heavy metal ions, *ACS Sens.*, 2023, **8**, 3812–3823.
13 M. A. Bujran, F. Dar, A. Tahir and B. Want, Terbium-doped metal-organic frameworks: Dielectric and ferroelectric properties with enhanced electrochemical sensing for heavy metal ion detection, *J. Solid State Chem.*, 2025, **341**, 125100.

14 C. Tian, Y. Lee, Y. Song, M. R. Elmasry, M. Yoon, D.-H. Kim and S.-Y. Cho, Machine-learning-enhanced fluorescent nanosensor based on carbon quantum dots for heavy metal detection, *ACS Appl. Nano Mater.*, 2024, **7**, 5576–5586.
15 Y.-L. Zhou, J. Song, L. Zhang, M.-F. Yin, M. Wu, B.-F. Duan and H.-P. Dai, Rare Earth complexes with dual functions for detecting Cu^{2+} ions and photocatalytic degradation of organic dyes: Synthesis, performance, and theoretical modeling, *J. Mol. Struct.*, 2025, **1337**, 142173.
16 W. Li, X. Liu, N. Lei, L. Liu, X. Li, H. Ren, J. Yin, L. Zhang, T. Yu and L. Fan, Zinc(II) organic framework based bifunctional biomarker sensor for efficient detection of urinary 5-Hydroxyindoleacetic acid and serum 3-Nitrotyrosine, *Spectrochim. Acta, Part A*, 2025, **329**, 125610.
17 X. Li, H. Ren, Y. Zhou, L. Liu, J. Wang, H. Hao, M. Muddassir and L. Fan, Stabilized Zinc(II) MOF based intelligent lumi nescent sensor for Ultrasensitive detection of 3-Nitrotyrosine biomarker in serum and tetracycline in food samples, *Microchem. J.*, 2025, **214**, 114134.
18 L. Liu, J. Yin, Y. Zhou, J. Liu, X. Li, H. Ren, H. Wang and L. Fan, Anionic PbMOF based yellow-emitting ratiometric luminescence sensor for efficient detection of styrene biomarker, *Microchem. J.*, 2026, **223**, 117327.
19 J. Wang, Y. Zhao, Y. Zhou, J. Liu, J. Yin, L. Zhang, H. Hao, X. Li and L. Fan, {Zn6Na} heptanuclear cluster based heterometallic framework as an intelligent luminescent sensor for efficient detection of carcinoid biomarkers, *Spectrochim. Acta, Part A*, 2026, 128015.
20 X. Li, H. Hao, L. Liu, H. Ren, J. Yin, J. Wang, L. Zhang, X. Zhang and L. Fan, Recent advances in metal–Organic framework-based luminescent sensors toward 3-nitrotyrosine biomarker, *Cryst. Growth Des.*, 2025, **25**, 7880–7902.
21 L. Xiao, T. Li, H. Ling, Y. Yang and S. Zhong, Construction of a dual colorimetric fluorescent imprinting polymer hybrid system for the detection of alpha-fetoprotein based on the multi- FRET effect and modeling of its color response mechanism, *Sens. Actuators, B*, 2024, **418**, 136264.
22 Y. Li, Y. Zhou, X. Liu, J. Lei, X. Qin, G. Li and Z. Yang, A NIR ratiometric fluorescence probe for rapid, sensitive detection and bioimaging of hypochlorous acid, *Spectrochim. Acta, Part A*, 2023, **302**, 123102.
23 S. Liu, S. Chen, L. Tian, Q. He, X. Wang, F. Lu and Y. Ning, A graphene-oxide-based fluorometric assay for norA gene transcription in MRSA using Nb. BbvCI-assisted target recycling and T7 exonuclease-triggered cascade dual recycling signal amplification, *Talanta*, 2023, **259**, 124549.
24 M. K. Goshisht, G. K. Patra and N. Tripathi, Fluorescent Schiff base sensors as a versatile tool for metal ion detection: strategies, mechanistic insights, and applications, *Mater. Adv.*, 2022, **3**, 2612–2669.
25 M. Z. Alam, Alimuddin and S. A. Khan, A review on Schiff base as a versatile fluorescent chemo-sensors tool for detection of Cu^{2+} and Fe^{3+} metal ion, *J. Fluoresc.*, 2023, **33**, 1241–1272.
26 S. Ramkumar, R. Kaviarasi, E. Kavyasri and G. S. Priyadarshini, A systematic investigation of luminescent Schiff bases: photophysical and DFT studies, *Chem. Phys. Impact*, 2023, **7**, 100294.
27 F. E. Ani, C. U. Ibeji, N. L. Obasi, M. T. Kelani, K. Ukogu, G. F. Tolufashe, S. A. Ogundare, O. E. Oyeneyin, G. E. Maguire and H. G. Kruger, Crystal, spectroscopic and quantum mechanics studies of Schiff bases derived from 4-nitrocinnamaldehyde, *Sci. Rep.*, 2021, **11**, 8151.
28 A. Kathiravan, K. Sundaravel, M. Jaccob, G. Dhinagaran, A. Rameshkumar, D. Arul Ananth and T. Sivasudha, Pyrene Schiff base: photophysics, aggregation induced emission, and antimicrobial properties, *J. Phys. Chem. B*, 2014, **118**, 13573–13581.
29 N. Kumari, S. Singh, M. Baral and B. Kanungo, Schiff bases: a versatile fluorescence probe in sensing cations, *J. Fluoresc.*, 2023, **33**, 859–893.
30 M. Köse, S. Purtas, S. A. Güngör, G. Ceyhan, E. Akgün and V. McKee, A novel Schiff base: Synthesis, structural characterisation and comparative sensor studies for metal ion detections, *Spectrochim. Acta, Part A*, 2015, **136**, 1388–1394.
31 Y.-W. Sie, C.-F. Wan and A.-T. Wu, A multifunctional Schiff base fluorescence sensor for Hg^{2+}, Cu^{2+} and Co^{2+} ions, *RSC Adv.*, 2017, **7**, 2460–2465.
32 Y. Pang, D. Meng, J. Liu, S. Duan, J. Fan, L. Gao and X. Long, Schiff base compounds as fluorescent probes for the highly sensitive and selective detection of Al^{3+} ions, *Molecules*, 2023, **28**, 3090.
33 A. A. A. Aziz and A. M. Abdel-Aziz, Asymmetric Schiff base-based colorimetric and fluorescent sensor for Al^{3+} detection in real samples and live-cell bioimaging, *RSC Adv.*, 2025, **15**, 16999–17014.
34 J. Fan, S. Zhang, Y. Xu, N. Wei, B. Wan, L. Qian and Y. Liu, A polyethylenimine/salicylaldehyde modified cellulose Schiff base for selective and sensitive Fe^{3+} detection, *Carbohydr. Polym.*, 2020, **228**, 115379.
35 S. Mondal and N. Dey, Polyethyleneimine-derived fluorescent conjugate for trace-level detection of multiple ions via signal amplification, *J. Photochem. Photobiol., A*, 2024, **455**, 115686.
36 S. Mondal and N. Dey, Modulating fluorescent responses in organic-doped polyethylenimine composites: Impact on pyrophosphate detection and biogenic phosphate analysis, *ACS Appl. Polym. Mater.*, 2024, **6**, 10242–10253.
37 D. Peralta-Domínguez, M. Rodríguez, G. Ramos-Ortíz, J. L. Maldonado, M. A. Meneses-Nava, O. Barbosa-García, R. Santillan and N. Farfán, A Schiff base derivative from cinnamaldehyde for colorimetric detection of Ni^{2+} in water, *Sens. Actuators, B*, 2015, **207**, 511–517.
38 I. Lee, S. Kim, S.-N. Kim, Y. Jang and J. Jang, Highly fluorescent amidine/Schiff base dual-modified polyacrylonitrile nanoparticles for selective and sensitive detection of copper ions in living cells, *ACS Appl. Mater. Interfaces*, 2014, **6**, 17151–17156.
39 C. Li, L. Xiao, Q. Zhang and X. Cheng, Reaction-based highly selective and sensitive monomer/polymer probes with Schiff base groups for the detection of Hg^{2+} and Fe^{3+} ions, *Spectrochim. Acta, Part A*, 2020, **243**, 118763.
40 T. Erkenez and M. Tümer, Polymer-anchoring Schiff base ligands and their metal complexes: Investigation of their

 This journal is © The Royal Society of Chemistry and the Centre National de la Recherche Scientifique 2026

electrochemical, photoluminescence, thermal and catalytic properties, *Arab. J. Chem.*, 2019, **12**, 2618–2631.
41 A. Chandra, A. A. Singh, S. Prasad, M. R. Andersson and D. Gedefaw, Crosslinking Approaches for Polyethylene Imine (PEI) and Its Uses in Adsorption of Heavy Metals, Dyes, and Carbon Dioxide, *Appl. Sci.*, 2025, **15**, 4767.
42 Z. M. Ayalew, X. Guo and X. Zhang, Synthesis and application of polyethyleneimine (PEI)-based composite/nanocomposite material for heavy metals removal from wastewater: A critical review, *J. Hazard Mater. Adv.*, 2022, **8**, 100158.
43 B. Robert and G. Nallathambi, Molecular entrapment of formaldehyde and filtering particulate matter using electrospun polyacrylonitrile/polyethylenimine nanofibers, *J. Polym. Res.*, 2022, **29**, 500.
44 N.-D. Tan, J.-H. Yin, G. Pu, Y. Yuan, L. Meng and N. Xu, A simple polyethylenimine-salicylaldehyde fluorescence probe: Sensitive and selective detection of Zn^{2+} and Cd^{2+} in aqueous solution by adding S2- ion, *Chem. Phys. Lett.*, 2016, **666**, 68–72.
45 S. Gulyuz and B. Kiskan, Combination of polyethylenimine and vanillin-based benzoxazine as a straightforward self-healable system with excellent film-forming ability, *Macromolecules*, 2024, **57**, 2078–2089.
46 G. H. Matar, E. Kaymazlar, M. Andac and O. Andac, Novel binary blended hydrogel films (chitosan-vanillin Schiff base/locust bean gum and Fe(III), Cu(II) & Zn(II) complexes):Synthesis, characterization, conductivity, and antibacterial activity, *J. Polym. Environ.*, 2023, **31**, 3509–3521.
47 R. Zhao, X. Yong, M. Pan, J. Deng and K. Pan, Aldehyde-containing nanofibers electrospun from biomass vanillin-derived polymer and their application as adsorbent, *Sep. Purif. Technol.*, 2020, **246**, 116916.
48 K. G. Kumar, K. S. John and R. Poduval, Polystyrene anchored vanillin Schiff base—Complexation and ion removal studies, *J. Appl. Polym. Sci.*, 2005, **98**, 1536–1539.
49 M. Jagannathan, D. Dhinasekaran, P. Soundharraj, S. Rajendran, D.-V. N. Vo, A. Prakasarao and S. Ganesan, Green synthesis of white light emitting carbon quantum dots: Fabrication of white fluorescent film and optical sensor applications, *J. Hazard. Mater.*, 2021, **416**, 125091.
50 S. Li, C. You, F. Yang, G. Liang, C. Zhuang and X. Li, Interfacial Mo–S bond modulated S-scheme $Mn_{0.5}Cd_{0.5}S$/Bi_2MoO_6 heterojunction for boosted photocatalytic removal of emerging organic contaminants, *Chin. J. Catal.*, 2025, **68**, 259–271.
51 C. Wang, K. Rong, Y. Liu, F. Yang and S. Li, Carbon quantum dots-modified tetra (4-carboxyphenyl) porphyrin/BiOBr S-scheme heterojunction for efficient photocatalytic antibiotic degradation, *Sci. China Mater.*, 2024, **67**, 562–572.
52 S. Nagar, S. Raizada and N. Tripathee, A review on various green methods for synthesis of Schiff base ligands and their metal complexes, *Results Chem.*, 2023, **6**, 101153.
53 A. L. Berhanu, I. Mohiuddin, A. K. Malik, J. S. Aulakh, V. Kumar and K.-H. Kim, *et al.*, A review of the applications of Schiff bases as optical chemical sensors, *TrAC, Trends Anal. Chem.*, 2019, **116**, 74–91.
54 L. Yu, L. Wang, H. Li, P. Li, H. Liu, M. Liu, J. Zhang, W. Wei and S. Li, Ti-Cl bond induced fast electron transfer in OH-regulated SrBi4Ti4O15/BiOCl for enhanced piezophotocatalytic antibiotic degradation, *Chin. Chem. Lett.*, 2025, 112228.
55 S. Li, Y. Zhao, X. Zhang, Y. Liu, T. Liu, W. Li, Y. Hou, W. Jiang and B. Zhang, Floatable S-scheme Bi4O5Br2/C3N4/carbon fiber cloth with robust internal electric field for efficient photocatalytic antibiotic decontamination, *Adv. Fiber Mater.*, 2025, **7**, 2032–2047.
56 K. Rajimon, A. Y. Alzahrani, D. S. R. Nair, D. P. Venkatesh and R. Thomas, Exploring the structure and dynamics of a fluorescent Schiff base (1E, 1E)-1, 1-(1,4-phenylene) bis (N-(4-chlorophenyl) methamine: Synthesis, spectroscopic analysis, thermal, electronic and crystallographic study with biological applications, *J. Mol. Struct.*, 2024, **1312**, 138546.
57 K. Fan, X. Wang, Y. Ma, Y. Li, G. Han, Z. Yin and J. Song, Water-soluble lanthanide coordination polymers particles with white-light emission and color tuning, *RSC Adv.*, 2019, **9**, 32137–32140.
58 T. Kotnik, G. Žerjav, A. Pintar, E. Žagar and S. Kovacic, Azineand imine-linked conjugated polyHIPEs through Schiff-base condensation reaction, *Polym. Chem.*, 2022, **13**, 474–478.
59 P. Nitschke, B. Jarzabek, A.-E. Bejan and M.-D. Damaceanu, Effect of protonation on optical and electrochemical properties of thiophene–phenylene-based Schiff bases with alkoxy side groups, *J. Phys. Chem. B*, 2021, **125**, 8588–8600.
60 J. Wang, Q. Meng, Y. Yang, S. Zhong, R. Zhang, Y. Fang, Y. Gao and X. Cui, Schiff base aggregation-induced emission luminogens for sensing applications: a review, *ACS Sens.*, 2022, **7**, 2521–2536.
61 R. C. Silva, F. S. Canisares, A. M. Mutti, A. M. Pires and S. A. Lima, Small Schiff base molecules derived from salicylaldehyde as colorimetric and fluorescent neutral-to-basic pH sensors, *Dyes Pigm.*, 2023, **213**, 111191.
62 S. Zheng and G. Liu, Polymeric Emissive Materials Based on Dynamic Covalent Bonds, *Molecules*, 2022, **27**, 6635.
63 S. K. Schoustra, V. Asadi and M. M. J. Smulders, Probing the Solubility of Imine-Based Covalent Adaptable Networks, *ACS Appl. Polym. Mater.*, 2023, **5**, 7798–7810.
64 Y. Chen, J. W. Lam, R. T. Kwok, B. Liu and B. Z. Tang, Aggregation-induced emission: fundamental understanding and future developments, *Mater. Horiz.*, 2019, **6**, 428–433.
65 S. S. Kumar, K. Vidhya, T. Thomas and S. K. Kalpathy, FTIRBased, Drop Cast, Wide Concentration Window Polymeric Sensor for Cu^{2+}(aq) Detection, *Polym. Adv. Technol.*, 2025, **36**, e70365.
66 S. Khan, M. Muhammad, H. M. Al-Saidi, A. A. Hassanian, W. Alharbi and K. H. Alharbi, Synthesis, characterization and applications of Schiff base chemosensor for determination of Cu^{2+} ions, *J. Saudi Chem. Soc.*, 2022, **26**, 101503.
67 M. Ali, H. Ullah, R. Khan, N. U. Islam, E. Khan, M. Ahmad, A. Ullah, A. Begum, G. Ali and Y. Xie, Unveiling the chemistry of polynuclear copper complexes: current synthetic strategies, properties and emerging applications, *RSC Adv.*, 2026, **16**, 2816–2849.

68 X. Liu, J. Hao, J. Liu and H. Tao, *IOP Conf. Ser.: Earth Environ. Sci.*, 2018, 012063.
69 C. Ni, W. Lu, J. Zhang, L. Peng, D. Xie and J. Ni, Blue-light emitting aminated pectin for detecting Cu^{2+} ion, *Int. J. Biol. Macromol.*, 2021, **176**, 272–281.
70 C. Zong, K. Ai, G. Zhang, H. Li and L. Lu, Dual-emission fluorescent silica nanoparticle-based probe for ultrasensitive detection of Cu^{2+}, *Anal. Chem.*, 2011, **83**, 3126–3132.
71 J. Harathi and K. Thenmozhi, AIE-active Schiff base compounds as fluorescent probes for the highly sensitive and selective detection of Fe^{3+} ions, *Mater. Chem. Front.*, 2020, **4**, 1471–1482.
72 M. Yang, D. Xu, W. Xi, L. Wang, J. Zheng, J. Huang, J. Zhang, H. Zhou, J. Wu and Y. Tian, Aggregation-induced fluorescence behavior of triphenylamine-based Schiff bases: the combined effect of multiple forces, *J. Org. Chem.*, 2013, **78**, 10344–10359.
73 L. Chen, X. Tian, C. Yang, Y. Li, Z. Zhou, Y. Wang and F. Xiang, Highly selective and sensitive determination of copper ion based on a visual fluorescence method, *Sens. Actuators, B*, 2017, **240**, 66–75.
74 Y. Wang, T. Chen, Z. Zhang and Y. Ni, Cytidine-stabilized copper nanoclusters as a fluorescent probe for sensing of copper ions and hemin, *RSC Adv.*, 2018, **8**, 9057–9062.
75 N. Shao, Y. Zhang, S. Cheung, R. Yang, W. Chan, T. Mo, K. Li and F. Liu, Copper ion-selective fluorescent sensor based on the inner filter effect using a spiropyran derivative, *Anal. Chem.*, 2005, **77**, 7294–7303.
76 T. Liu, D. Li, N. Li, W. Zhang and Y. Zhao, Ultrasensitive quantifying copper ions in serum by tapered optical fiber fluorescent sensor based on static quenching effect, *Sens. Actuators, B*, 2023, **396**, 134557.
77 K. Shanmugaraj and M. Ilanchelian, A ''turn-off'' fluorescent sensor for the selective and sensitive detection of copper(II) ions using lysozyme stabilized gold nanoclusters, *RSC Adv.*, 2016, **6**, 54518–54524.
78 C. Baslak and A. N. Kursunlu, A naked-eye fluorescent sensor for copper(II) ions based on a naphthalene conjugate Bodipy dye, *Photochem. Photobiol. Sci.*, 2018, **17**, 1091–1097.
79 Y. Li, L. Wang, L. Wang, B. Zhu and J. Ma, A novel carbazolebased fluorometric and colorimetric sensor for the highly sensitive and specific detection of Cu^{2+} in aqueous solution, *RSC Adv.*, 2023, **13**, 33276–33287.
80 Y.-n Zhang, W. Liang, L. Li, H. Zhang, S. Cao, B. Han and Y. Zhao, Optical fiber fluorescence Cu^{2+} sensing technology based on CdSe/ZnS quantum dots: Large detection range, low detection limit, *Anal. Chim. Acta*, 2024, **1331**, 343300.
81 Y. Nakaya, T. Hirose, R. Tamori, N. Fujitake, S. Nakashima, H. Yamamura and H. Satoh, Solid-phase fluorescence excitation-emission matrix spectroscopy of soil, fulvic acid fractions, and clay mineral complexes: Evidence from red shift of fluorescence maxima associated with aggregation, *Environ. Res.*, 2025, 121900.
82 Y. Li, H. Lin, C. Luo, Y. Wang, C. Jiang, R. Qi, R. Huang, J. Travas-sejdic and H. Peng, Aggregation induced red shiftemission of phosphorus doped carbon dots, *RSC Adv.*, 2017, **7**, 32225–32228.

 This journal is © The Royal Society of Chemistry and the Centre National de la Recherche Scientifique 2026